Received: 13 January 2024 | Revised: 9 September 2024 | Accepted: 13 September 2024

DOI: 10.1002/esp.5999

RESEARCH ARTICLE

ESPL WILEY

Cosmogenic ^{10}Be- and ^{21}Ne-based model exposure ages of desert pavements in the Thar Desert, India

Rahul K. Kaushal[1] | Sukumar Parida[1] | Pavitra V. Kumar[2] | Pankaj Kumar[2] | Samuel Niedermann[3] | Robert J. Wasson[4] | Ram P. Dhir[5†] | Sundeep Chopra[2] | Sheila Mishra[6] | Shanti Pappu[6,7] | Ashok K. Singhvi[1]

[1]AMOPH Division, Physical Research Laboratory, Ahmedabad, India

[2]National Geochronology Facility, Inter University Accelerator Centre, New Delhi, India

[3]Deutsches GeoForschungsZentrum, Potsdam, Germany

[4]College of Science and Engineering, James Cook University, Cairns, 4232, Australia; Fenner School of Environment and Society, Australian National University, Canberra, Australia

[5]Retired Scientist, Central Arid Zone Research Institute, CAZRI Road, Jodhpur, India

[6]Sharma Centre for Heritage Education, No.4. School Road, Shollinganallur, Chennai, Tamil Nadu, 600119, India

[7]School of Interwoven Arts and Science, Krea University, Sri City, Andhra Pradesh, India

Correspondence
Rahul Kumar Kaushal, AMOPH Division, Physical Research Laboratory Ahmedabad, -380009, India.
Email: rahulkiitgn@gmail.com

Funding information
Department of Science and Technology-Scientific and Engineering Research Board (DST-SERB),, Grant/Award Number: DST-YOSCP grant no. SR/S9/YSCP-03/2019

Abstract

The Thar Desert, India has desert pavements comprising angular-subangular to well-rounded gravels at marginally higher elevations than the surrounding terrain. Sedimentological and geomorphic analyses suggest that the pavements are lags of weathered Mesozoic and older bedrock. The presence of Palaeolithic artefacts on the pavement surfaces and occasionally within their matrix was used to infer their antiquity and landscape stability.

This study presents the first surface exposure ages based on cosmic-ray-produced ^{10}Be and ^{21}Ne for pavements at four sites in the Thar Desert, viz. Bhojka, Hamira, Solanki and Jayal. The computation of model exposure ages assumed that (a) the gravels were derived from cemented conglomerates, uplifted by tectonics and thereafter disintegrated by climate, and (b) cosmogenic nuclide production in the gravels began when the conglomerates approached the surface and, continued during their disintegration, gravity sliding of individual gravels and storage, until the present. Assuming an average burial depth of 50 cm, ^{21}Ne and ^{10}Be data provide ages ranging from 1.30 to 2.92 Ma and 1.11 to 5.4 Ma, respectively, for the two nuclides.

Published electron spin resonance ages of Thar calcretes suggest the presence of water and extreme seasonality since 1.54 Ma. Such conditions facilitated the mobilization and precipitation of carbonates. The pavement ages and the minimum age of the conglomerate at 2.51 Ma extend the time of such desertic conditions to > 2.51 Ma and suggest that the initiation of desertic conditions in the Thar was possibly linked to global aridity beginning around 3.6 Ma.

Depending on assumptions, cosmic ray surface exposure (^{10}Be) ages at Jayal range between 0.76 and 2.43 Ma. In the context of the Indian Palaeolithic, the presence of tools on the gravel surfaces and within dunes, suggests frequent occupation of this region from at least 0.76 Ma and, parallels Early to Middle Pleistocene Acheulian assemblages from Southern India.

KEYWORDS

^{10}Be and ^{21}Ne, cosmic ray exposure ages, desert pavement, Palaeolithic, Thar Desert

† deceased

1 | INTRODUCTION

1.1 | Desert pavements

In arid environments, desert pavements are mappable anomalous geomorphic features, which reflect arid/hyper-arid phases that assist their formation and preservation over long durations (Fitzsimmons et al., 2013; Pietsch & Kuhn, 2012). Conditions for their preservation include minimal erosion, low slope angles and minimal bioturbation. Fujioka & Chappell (2011) and Seong, Dorn, & Yu (2016) presented global reviews of the time scales of desert pavements using chronologies, mostly based on cosmogenic radionuclides. Important regional studies are (a) the Atacama in Chile (Dunai, López, & Juez-Larré, 2005; Evenstar et al., 2009; Nishiizumi et al., 2005; Wang et al., 2015), (b) the Gibber plains in Australia (Fujioka et al., 2005), (c) the southern Levant in Israel (Amit et al., 2011; Matmon et al., 2009), (d) the Gobi in China (Lü et al., 2010) and (e) the Thar Desert in India (Moharana & Raja, 2016; Rajaguru, Mishra, & Ghate, 1996).

In the Thar Desert, gravelly pavements occur over an area spanning up to approximately 10,000 km^2. Key localities are observed at Bhojka, Hamira near Jaisalmer, Solanki near Barmer and Jayal near Nagaur (Figure 1). The sites at Jayal and Bhojka have Palaeolithic artefacts which provide a minimum age for the gravel (Misra et al., 1979 and references therein; Misra & Rajaguru, 1989; Misra, 2006, 2007).

The genesis of these gravels has been widely debated. Early studies suggested that the gravel pavements near Nagaur-Jayal are of post-Vindhyan to recent age (i.e., < 1,200 Ma, Hackett, 1880). Later studies considered the gravels as evidence for rivers and mega-floods that do not exist anymore (Agrawal et al., 1980; Bakliwal & Grover, 1988; Ghosh, 1977; Oldham, 1983; Tiwari, 1992). Fluvio-glacial processes were also suggested based on the presence of surface striations, grooves, polished clast surfaces and heterogeneity of gravel size (Biswas & Ghosh, 1981; Mukhopadhyay & Ghosh, 1976). It is now generally considered that these gravels are desert pavements and have been formed through autochthonous weathering of

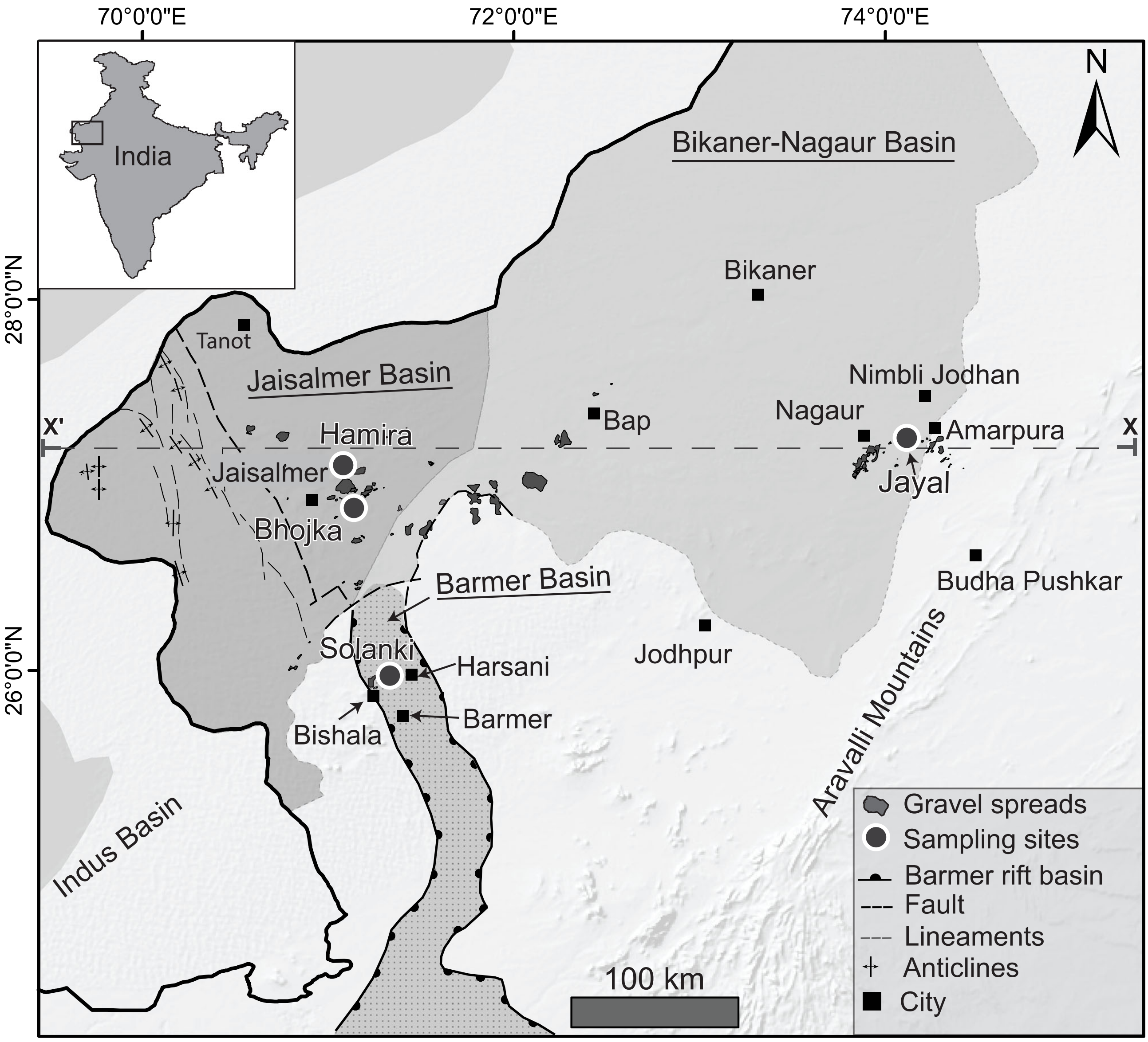

FIGURE 1 Hillshade image of the study area showing three major sedimentary basins of the Thar Desert in India, its geomorphological features, and the spatial distribution of gravel spread pavements (see Figure S2). The Thar is limited by the Indus Basin and the Aravalli Mountains. Sedimentary basin boundaries are adopted from Wadhawan (2018) and National Data Repository, Directorate General of Hydrocarbons (DGH), Ministry of Petroleum and Natural Gas, Government of India (https://www.ndrdgh.gov.in/NDR/?page_id=656).

conglomerates of Mesozoic and older geological phases (Rajaguru, Mishra, & Ghate, 1996; Sharma, 1987).

The gravel spreads originated from sedimentary sequences deposited within the Jaisalmer, Bikaner-Nagaur and Barmer Basins (Wadhawan, 1988, 2018; Roy & Jakhar, 2002; Figure 1). Deposition of gravel-bearing conglomerates was episodic and their stratigraphic ages range from the Mid Miocene to the Pleistocene in the Barmer Basin; the Mesozoic in the Jaisalmer Basin, and the Permian-Carboniferous to the Pleistocene in the Bikaner-Nagaur Basin (Wadhawan, 1988, 2018; Roy & Jakhar, 2002; see Table S1). Previous studies based on geological and geophysical investigations identified lineaments that were linked to horst and graben structures on the west Rajasthan shelf (Brahmam, 1993; Roy & Jakhar, 2002; Sinha Roy, 1986; Wadhawan, 1988) as well as in the Luni Basin, Eastern Thar (Bajpai, 2004).

The Aravalli Mountains supplied sediments to the three sedimentary basins located to their west and created alluvial fans with undulating topography (Wadhawan, 1988, 2018; Roy & Jakhar, 2002 and references therein; Figure 1). Fan sediments were later cemented by carbonates and iron oxides. Subsequent tectonic activity associated with the lineaments uplifted the sediments and exposed them to denudation by sub-aerial processes (Rajaguru, Mishra, & Ghate, 1996; Wadhawan, 2018). Cemented conglomerates that approached the surface lost their matrix and disintegrated over time, providing loose gravels which were redistributed through gravity sliding, creating a surface layer of loose clasts, now termed desert pavements (Adelsberger et al., 2013; Knight & Zerboni, 2018; Rajaguru, Mishra, & Ghate, 1996).

1.2 | Pavement chronology: present status

The gravels at Nagaur and Jayal were assigned a late Neogene age based on fossil wood (Ganjoo et al., 1984). At and around Jayal (Misra, 2007; Misra et al., 1980), Palaeolithic tools were discovered on the surface of the gravel and occasionally within. These studies proposed a long-term stability of these gravels and the entire landscape with repeated occupation of the region by successive prehistoric populations that were attracted by the abundance of raw material (Allchin, Goudie, & Hegde, 1978; Agrawal et al., 1980; Misra et al., 1979 and references therein, Misra et al., 1980, 1982, Misra, 2006, 2007, Misra & Rajaguru, 1989, Rajaguru, Mishra, & Ghate, 1996). At Amarpura, in this region, electron spin resonance (ESR) ages on carbonates exceed 797 ka (Kailath et al., 2000). Gaillard et al. (2010) considered that this age estimate could be used to date the Acheulian at Amarpura in the Thar Desert. Overall in India, the Acheulian dates to the Early Pleistocene [Attirampakkam, ~1.7–1.1 Ma (Pappu et al., 2011); Isampur ~1.2 Ma (Mishra et al., 2010; Paddayya et al., 2002) and several sites in Western India (Gaillard et al., 2010; Mishra et al. 2010; Sangode et al., 2007)]; while the early Middle Palaeolithic begins at ~380–200 ka (Akhilesh et al., 2018; Anil et al., 2022; Blinkhorn et al., 2021; Singhvi et al., 2010).

This study aims to further the understanding of the event chronology of the evolution of the Thar by providing model surface exposure ages of gravelly pavements, using in-situ produced cosmogenic ^{10}Be and ^{21}Ne.

2 | GEOLOGY AND GEOMORPHOLOGY

The Thar Desert is bounded between the Aravalli Mountains and the Indus basin (~25–30°N and ~70–76°E) and comprises diverse landforms such as sand dunes, sand sheets, alluvial flats, fluvial channels, rocky pediments and lakes (Dhir, Joshi, & Kathju, 2018; Singhvi & Kar, 1992). The basement comprises granite, rhyolite and gneiss. Most of the sedimentary record of the Thar is preserved in three sedimentary basins with up to ~200–350 m sediment piles, resting on rocks of the Precambrian and Mesozoic eras (Bakliwal & Wadhawan, 2003; Roy & Jakhar, 2002; Singhvi & Kar, 1992; Sinha Roy, Malhotra, & Mohanty, 1998; Wadhawan, 1988, 2018). Sedimentation in these basins, viz. Bikaner-Nagaur, Jaisalmer and Barmer began during the Proterozoic (Figures 1 and S1) under fluvial, continental and shallow marine environments (Table S1) and produced alternating sequences of pebbly sandstone, conglomerate and limestone (Bakliwal & Wadhawan, 2003; Bhandari, 1999; Das Gupta, 1975; Dolson et al., 2015; Roy & Jakhar, 2002). Marine or littoral environments prevailed during the Eocene to the late Tertiary (Dhir, 1976; Misra, 1961; Misra et al., 1982). Thereafter, tectonics and retreat of the sea during the late Tertiary exposed the basin sediments to subaerial weathering, erosion and re-deposition (Misra, 1961).

Palaeoenvironmental data for the Thar during the mid-late Quaternary has been summarized in Singhvi (2004). The widespread presence of calcretes of varied forms and contexts suggests that the Thar region experienced a semi-arid to arid climate with accentuated seasonality, which enabled the mobilization of carbonates and the precipitation of calcretes. ESR ages of calcretes near the Jayal area (from Katoti village) and Nimbli-Jodhan suggest that such conditions existed from 1.54 ± 0.15 to 0.84 ± 0.07 Ma (Dhir et al., 2004; Kailath et al., 2000). Desiccation increased with time, and during the late Quaternary widespread evidence of aeolian activity with intermittent phases of fluvial episodes is recorded (Bajpai, 2004; Dhir et al., 2010; Dhir & Singhvi, 2012; Jain et al., 2005; Jain & Tandon, 2003; Misra et al., 1980; Singhvi, 2004; Singhvi & Kar, 2004).

3 | FIELD OBSERVATIONS

Gravel occurrences reviewed by Rajaguru, Mishra, & Ghate (1996) were revisited, remapped using Google Earth satellite imagery and verified in the field (Figures 1 and S2). Sites at Bhojka, Hamira near Jaisalmer, Solanki near Barmer and Jayal near Nagaur and others cover ~ 10,000 km^2 area (Figures 1 and 2). These were sampled for cosmogenic nuclide-based chronology, and sediment attributes comprising clast sizes, clast orientation and depth profiles were documented. A brief account of each of these sites is given below.

3.1 | Bhojka

This gravel spread extends laterally over several kilometres (~23 km^2; Figure 2) and at places forms an ~ 9 m thick, gently rounded ridge (Dhir et al., 1992; Rajaguru, Mishra, & Ghate, 1996). Surface gravels have a b-axis (intermediate axis used for width measurements) ranging from 1 to 8 cm. The gravels comprise large pebbles, occasional

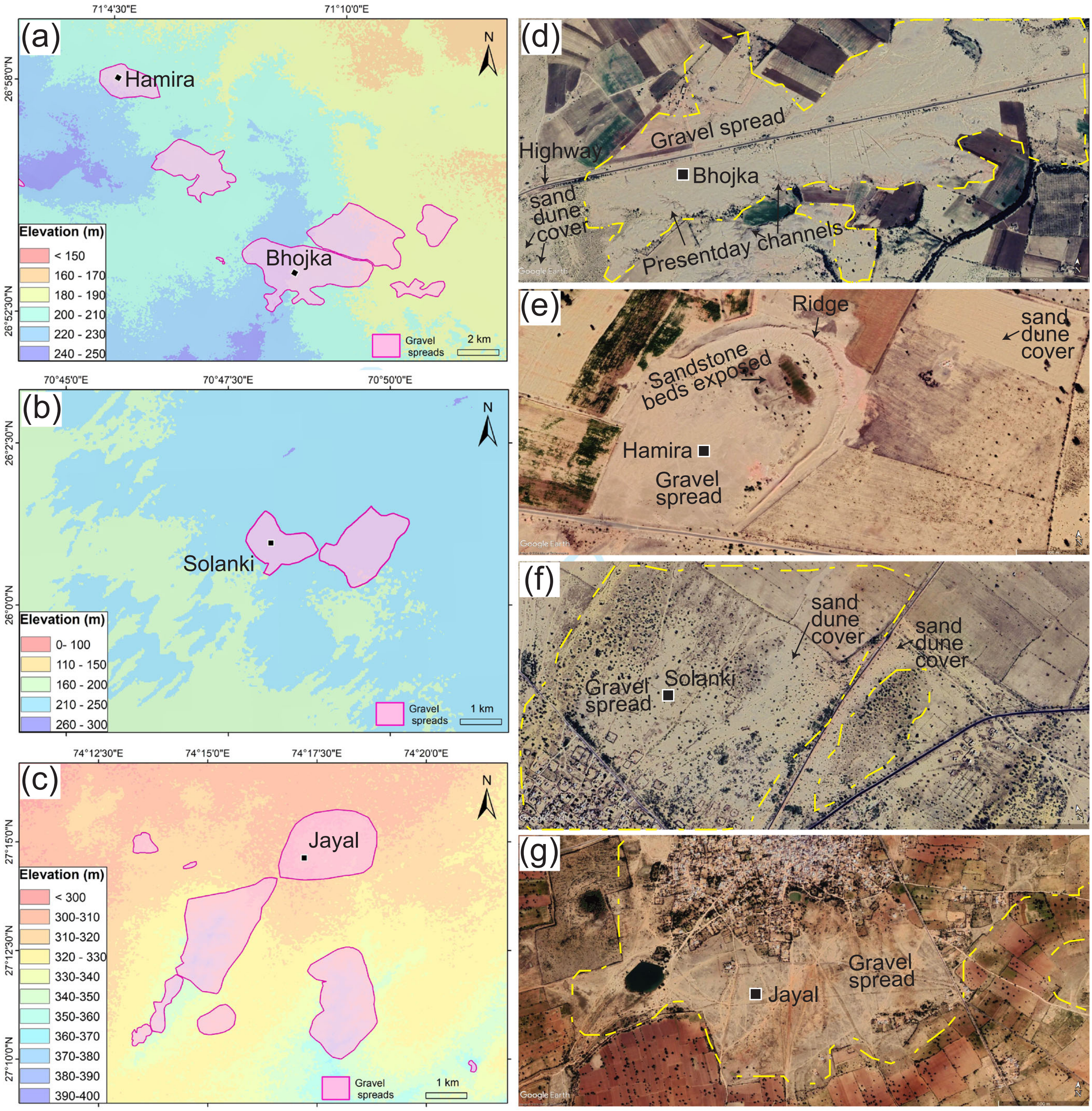

FIGURE 2 Spatial distribution of gravel spread sites across the Thar Desert. (a-c) Gravel spread sites (Bhojka, Hamira, Solanki and Jayal) are overlaid on the digital elevation model to show topographic variations. (d-g) Google satellite images of these four sites provide synoptic, zoomed-in subsets of gravel spreads, showcasing their surface characteristics.

cobbles and rare boulders of siliceous rocks with occasional angular slabs of local ferruginous sandstone, brown limestone, calcrete, jasper, rhyolite and granite pebbles (Figure 3a-d). The gravels are moderately sorted. The base is cemented by calcrete resting on the sandstone and shale of the Lathi Formation (Roy & Jakhar, 2002; Figure 4).

3.2 | Hamira

The gravel spread at Hamira, ~10 km NW of Bhojka (Figure 2a), is a gently undulating terrain, comprising a 10–15 cm thick gravel layer draped over underlying bedrock. This site covers an area of ~3 km^2 (Figure 2a). Surface gravels have a b-axis ranging from 1 to 6 cm. Occasional quartz clasts are angular, possibly being broken fragments of larger boulders or pebbles. The gravels, comprising quartzites, are wind polished, well sorted and rounded to subrounded. To the north, a subdued hillock about 1 m high has scattered pebbles derived from ferruginous sandstone beds (Figure 2e). These locally add angular clasts and slabs to these gravels. The basal part of the gravel exhibits carbonate cementation and rests unconformably on sandstone and shale beds of the Lathi Formation of the Jurassic age (Kaila & Roy, 1989).

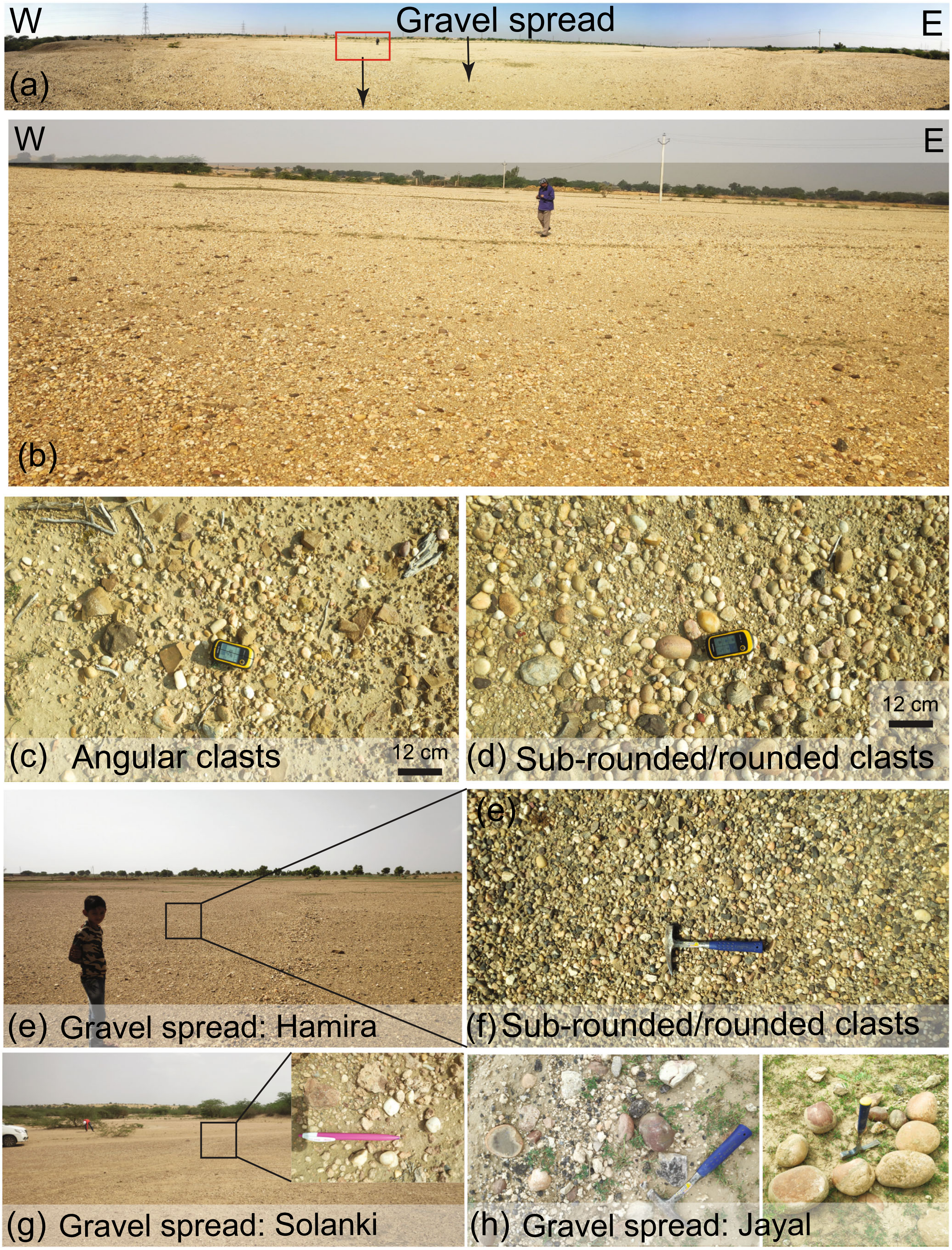

FIGURE 3 (a) Panoramic view of gravel spread at Bhojka; (b) Bhojka gravels show extensive spread (see person for scale); (c) presence of angular clasts released from local bedrock (sandstone and limestone); (d) sub-rounded/rounded clasts. (e-f) Hamira gravels show flat surface armouring by mosaic of highly resistant lithology. (g) Solanki gravel spread site shows sub-rounded/rounded pebbles and angular clasts of sandstone. (h) Jayal site shows boulders and gravel-sized clasts. A hand-held GPS, pen and hammer provide the scale.

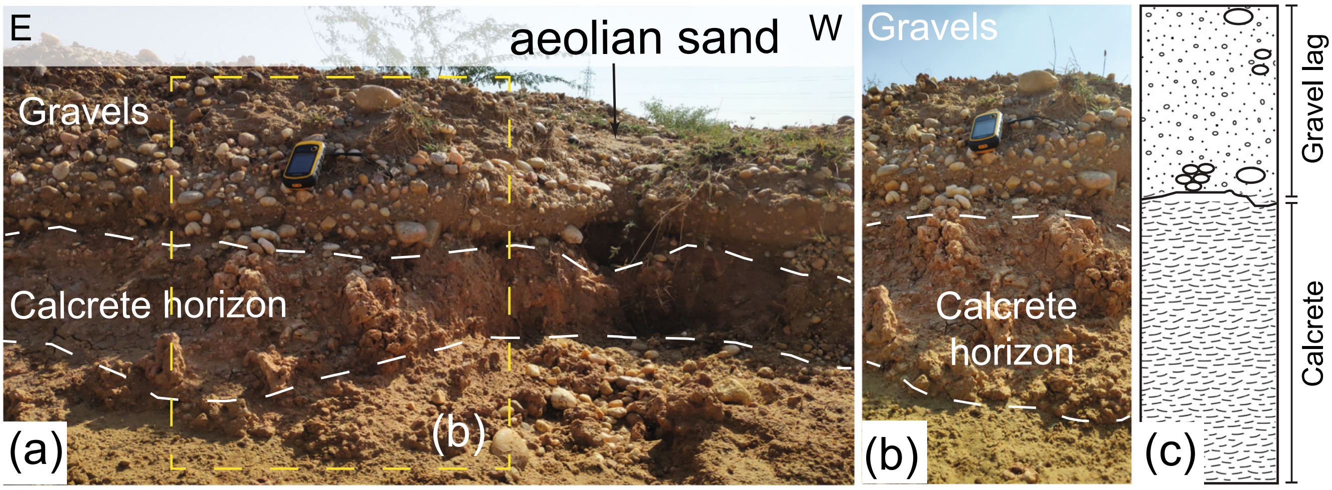

FIGURE 4 (a-b) Field pictures showing a section of the gravel spread at Bhojka; viewed from north. The gravels unconformably overlie the indurated hard-pan calcretes. A hand-held GPS provides the scale. (c) Schematic stratigraphic section to show gravels and calcrete. The section was exposed along a channel used for irrigation.

3.3 | Solanki

Near Barmer, gravel spreads typically 8–10 cm thick covering an area of ∼5 km^2. The accessible part of the gravel spread is limited due to a cover of aeolian sands. Two exposures at Bishala and Solanki were examined. The exposure at Bishala comprises angular to sub-angular metavolcanic rocks on flat terrain (Figure S3a-b). The gravel exposure at Solanki comprises pebbles, cobbles, angular sandstone clasts and angular sharp-edged granitic pieces (Figure 3g, S3c-f). The b-axis ranges from 1 to 4 cm for the surface gravel. These gravels occur as a thin (5–8 cm) sheet, derived from the erosion of sandstone and conglomerate rocks of the Fatehgarh Formation of Palaeocene age (Table S1). This formation comprises coarse-grained sandstone and conglomerate with pebbles of quartz and granite (Dolson et al., 2015; Sisodia & Singh, 2000).

3.4 | Jayal

At Jayal, a gravel spread covers an area of approximately 35 km^2 (Figure 2c) and exhibits a 40–70 m high gently rounded ridge (Dhir et al., 1992; Rajaguru, Mishra, & Ghate, 1996). It comprises a poorly sorted, boulder-cobble unit with a yellowish-brown, carbonate-cemented silty sand matrix. Rock types here include quartzite, vein quartz, quarzitic sandstone and schist. The disintegrated gravels and boulders at the Jayal site were classified as a part of a petromict conglomerate (Misra et al., 1980). It was also suggested earlier that the gravels were deposited through fluvial processes with the clasts being sourced from the Aravalli Mountains via streams. A more recent suggestion is that the Jayal conglomerate belongs to the Nagaur Group of the Marwar Supergroup and was tectonically exhumed during pre-Quaternary times (Wadhawan, personal communication).

4 | METHODS: SURFACE EXPOSURE DATING WITH COSMOGENIC NUCLIDES

4.1 | Sampling, quartz separation and ^{10}Be analysis

For each gravel deposit, 20–30 representative quartzite clasts were collected and processed for determination of the concentrations of cosmic ray-produced nuclides in quartz. Typically, clasts with their intermediate axis around 2–4 cm were chosen from an extended area of ∼ 1,000 m^2. In addition, a conglomerate specimen (BHCONG) was collected near Bhojka, and pebbles and granules from it were used for quartz extraction. The quartzite was milky-grey to white. A hand-held GPS provided the coordinates and the altitude. Topographic shielding was measured using a Brunton compass. The reason for combining several clasts into a single sample was the consideration that the conglomerates would have taken time to disintegrate into gravels and therefore individual gravel pieces may have had somewhat different individual exposure histories. Therefore, it was anticipated that mixing them together would provide an average exposure age. Such approaches have been used in cosmogenic nuclide studies to estimate the age of fluvial terraces, determination of inherited nuclide components (Anderson, Repka, & Dick, 1996; Hancock et al., 1999; Repka, Anderson, & Finkel, 1997) and to quantify average erosion rates of ridge crests in a tectonically active region (Heineke et al., 2019 and references therein).

The choice of the nuclides ^{10}Be and ^{21}Ne was based on the fact that ^{21}Ne is a stable nuclide, which would provide the integrated (total) exposure history of the samples, while the radionuclide ^{10}Be has a half-life of 1.387 Ma (Chmeleff et al., 2010; Korschinek et al., 2010), and its decay during times of reduced (or no) cosmogenic nuclide production would reveal possible occurrences of overburden, such as migrating aeolian sands. Together, these nuclides were expected to provide an estimate of the time since the gravels approached and remained within a few metres of the surface.

Samples were crushed and sieved to 250–500 μm grain size for chemical processing at the Physical Research Laboratory (PRL), Ahmedabad. Pure quartz extraction, ^{10}Be sample preparation and AMS measurements were then conducted in the Geochronology Laboratory at the Inter-University Accelerator Centre (IUAC) in New Delhi, India, following the standard methods described by Kohl & Nishiizumi (1992). Detailed procedures for chemical processing and AMS measurements are provided as supplementary online material (Text S1).

4.2 | Neon isotopic analysis and cosmogenic ^{21}Ne determination

The neon isotopic composition was measured on a subset of purified quartz samples in the noble gas laboratory of the Deutsches GeoForschungsZentrum (GFZ) in Potsdam. Quartz fragments were crushed to ~100 μm grain size to minimize the contribution of trapped Ne from fluid inclusions and to ensure complete extraction of cosmogenic Ne at 800°C (Niedermann, 2002). Samples were wrapped in aluminium foil and baked at 100°C for a week under vacuum to remove adsorbed atmospheric gases. Extraction of noble gases comprised stepwise heating at 400°C, 600°C, 800°C and 1,200°C in an ultra-high vacuum furnace. Neon isotopic data were corrected for instrumental mass fractionation, isobaric interferences and analytical blanks. Error limits are shown at the 1σ confidence level and include statistical uncertainties of the measurement, uncertainties of the sensitivity as well as blank and interference corrections. The analytical procedures and data reduction methods followed Niedermann, Bach, & Erzinger (1997).

In quartz, cosmic ray-produced Ne has a characteristic ^{22}Ne/^{21}Ne ratio. In a three-isotope diagram; a two-component mixture of cosmogenic Ne and a trapped Ne component (such as atmospheric Ne) must plot on the spallation line (Niedermann, 2002; Niedermann, Graf, & Marti, 1993). In this study, gas extractions by in vacuo crushing of samples (giving the composition of Ne trapped in fluid inclusions) yielded ^{22}Ne/^{20}Ne ratios lower and ^{21}Ne/^{20}Ne ratios slightly higher than air (^{22}Ne/^{20}Ne = 0.1020 and ^{21}Ne/^{20}Ne = 0.002959; see Table S3), suggesting a trapped Ne component that is fractionated and contains a small contribution from crustal Ne.

The 400°C, 600°C and 800°C data are consistent with the mixing of a trapped Ne component with cosmogenic Ne (a mixing line parallel to the spallation line through the air that is shown in Figure S4), though the fractionation observed in the heating steps was somewhat higher than for the crushing extractions. Cosmogenic ^{21}Ne concentrations were calculated as the total ^{21}Ne excess in the 400°C, 600°C and 800°C heating steps compared to the respective trapped Ne composition as determined by crushing extractions and are given in 10^6 atoms/g, with 1σ errors in Table 2.

4.3 | Calculation of the exposure ages

The concentration of cosmogenic nuclides in a sample depends on the net cosmic ray flux and the duration of exposure (Lal, 1991). Calculation of an exposure age requires (a) the cosmogenic nuclide concentration (corrected for topographic shielding) and (b) the production rate, which varies with depth in the sediment matrix, latitude and elevation (e.g. Granger & Smith, 2000; Lal, 1991; Niedermann, 2002; Vermeesch, 2007).

Under the assumption of zero erosion and no burial the following equation provides a minimum ^{10}Be exposure age (t),

$$t = -\frac{1}{\lambda}\ln\left(1-\frac{N\lambda}{PS}\right) \tag{1}$$

where N is the nuclide concentration (atoms/g), P is the surface production rate (in atoms/g/a) at the sampling location, t is exposure age, λ is the decay constant of a radionuclide (λ = 0 for stable nuclides) and S is the shielding factor. Under similar assumptions of no erosion and no burial, the minimum ^{21}Ne exposure age can be calculated using

$$t = \frac{N}{PS} \tag{2}$$

Under the assumption of a constantly eroding surface, the following equation provides the minimum exposure age for ^{10}Be and ^{21}Ne,

$$t = -\frac{1}{\lambda+\frac{\rho\varepsilon}{\Lambda}}\ln\left(1-\frac{N}{PS}\left(\lambda+\frac{\rho\varepsilon}{\Lambda}\right)\right) \tag{3}$$

where ϵ is the erosion rate (cm/yr), Λ is the spallogenic neutron attenuation length (g/cm^2) and ρ is the rock density (g/cm^3). λ = 0 for stable nuclides.

Calculated exposure ages based on equations (1), (2) and (3) provide minimum exposure ages (Gosse & Phillips, 2001; Lal, 1991; Niedermann, 2002).

^{10}Be and ^{21}Ne model exposure ages were computed by using Equations 1, 2 and 3 along with Lal's (1991) production rate scaling factors. Only the spallation production mechanism was considered and the following parameters were used:

a. A ^{10}Be half-life of 1.387 Ma (Chmeleff et al., 2010; Korschinek et al., 2010),
b. A sea level/high latitude ^{10}Be production rate (P_{SLHL}) of 4.01 atoms/g/a (Borchers et al., 2016),
c. A sea level/high latitude ^{21}Ne production rate (P_{SLHL}) of 17.8 atoms/g/a obtained by combining the ^{10}Be production rate given above and the ^{21}Ne/^{10}Be production ratio according to Fenton et al. (2019),
d. A rock density (quartz) of 2.65 g/cm^3,
e. An attenuation length of ^{10}Be and ^{21}Ne of 160 g/cm^2 was used to calculate the depth dependence of production rates,
f. During their entire antiquity, the samples were within 200–300 m of the surface and therefore thermal diffusion loss of cosmogenic ^{21}Ne due to the geothermal gradient (Ben-Israel et al., 2018) was not considered.

To estimate the exposure age of the gravel mixture, we considered four scenarios (see section 5.2) presented in Table 3, where individual pebbles would have had a varied production rate history. Among them, as a simplifying assumption, an average depth of 50 cm was used to estimate a shielding factor (S) of 0.44 using $S = e^{-\frac{\rho Z}{\Lambda}}$ (Gosse & Phillips, 2001). Here, Λ is the spallogenic neutron attenuation length (g/cm^2), ρ is the rock density (g/cm^3) and Z is the depth of the sample

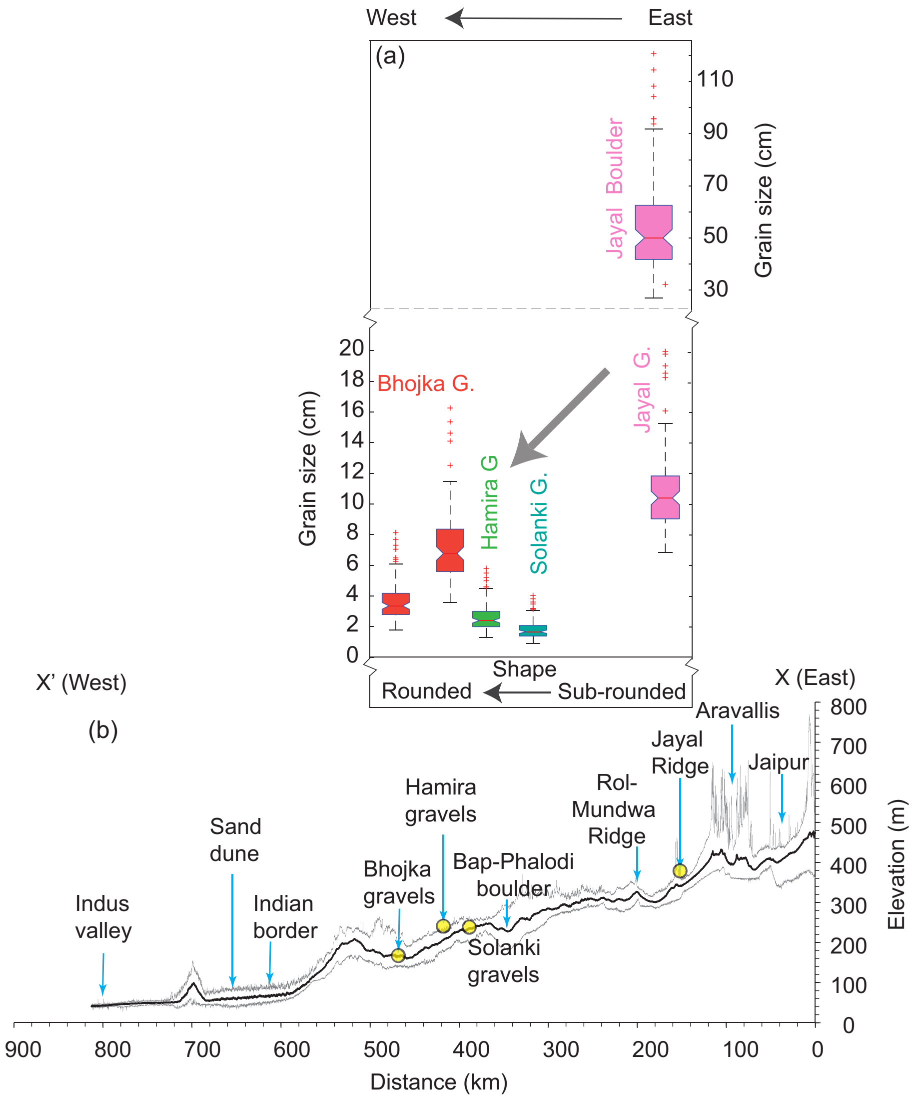

FIGURE 5 (a) Spatial distribution of gravel clast size from the studied sites is projected onto a swath profile to illustrate the reduction in gravel size due to sediment transport during the Mesozoic era. The grey arrow indicates that clast size reduces from the Jayal area (east) to the Jaisalmer area (west). (b) Swath profile shows present-day topographic variation and the regional slope from east to west across the desert. Profile X-X' (see Figure 1 for location) provides minimum, maximum and mean elevation (solid black line). The elevations were extracted from SRTM 30 m DEM data in an 800 $\times$ 200 km window.

TABLE 1 Geomorphic expression of gravel spreads in the Thar desert: field observations.

Sl. No.	Site	Terrain type	Lithology	Size and shape	Geomorphic features	Possible source
1	Bhojka, near Jaisalmer	Eastern side of the ridge, flat, occasional undulating	Quartz, quartzite, calcrete, granitic pebbles, dolerite, obsidian, conglomerates	Sub-rounded to oblong-shaped 1 cm to 8 cm gravel size, moderately sorted	Wind abrasion, polishing surfaces, grooves in bedrock	Bedrock Lathi Formation-Conglomerate beds
2	Hamira, near Jaisalmer	Flat terrain	Quartz, quartzite, angular sandstone slabs	Sub-rounded, 1 cm to 6 cm in size, well sorted	Wind abrasion	Nearby hill top Bedrock Lathi Formation-Conglomerate beds
3	Solanki, near Harsani town	Flat terrain with undulating surface	Quartz, quartzite, obsidian, metavolcanics angular clasts	Sub-rounded, pebbles-cobbles, 1 cm–4 cm size pebbles	Slightly orientated to wind direction	Fatehgarh, Sarnu Fm. Sandstone
4	Jayal, near Nagaur	Undulating surface with deep valleys and gullies	Quartz, quartzite	Rounded to sub-rounded, boulder size, poorly sorted, 6 cm to 80 cm	Fluvially modified, occur as ridges	Nagaur group of rocks, Kolayat Fm. with conglomerate
5	Bishala	Flat sandy plain	Obsidian, metavolcanics angular clasts	Angular-subangular, poorly sorted, 4 cm to 12 cm	Wind abrasion, pores contain aeolian sand	Sarnu Fm, Cretaceous volcanics

below the surface (in cm). This shielding factor was used to obtain a model exposure age of the gravel mixture.

5 | RESULTS AND DISCUSSION

5.1 | Gravels: spatial distribution, clast, matrix and provenance

The spatial distribution of gravel pavements across the Thar Desert provides insights into regional geomorphological processes. These sites were overlaid onto a digital elevation model (DEM) to analyse their topographic variations (Figure S2). At Bhojka and Hamira, gravel spreads range from 200 to 230 m in elevation, while the Solanki gravels span 210 to 250 m (Figure 2a, b). Jayal, however, is located at an elevation between 300 and 350 m (Figure 2c).

This spatial distribution of gravel spreads was projected onto an east–west swath profile in Figure 5, showing a decrease in gravel size from east to west, which has been attributed to sediment transport processes during the Mesozoic or earlier era (Misra et al., 1980; Rajaguru, Mishra, & Ghate, 1996). Across an east-to-west distance of ~350 km, the mean clast size decreases from 11 to 3 cm and the roundness (ratio of mean minor to major axis) increases from 0.64 to 0.75 (Figure 5, Table 1).

Similarities of lithologies between sites (comprising quartzite, schist and arenaceous rocks) and the E-W regional slope suggest the same source for all gravel spreads, i.e., the Aravalli Mountains. This is the only mountain chain that could supply the material that was most likely deposited as a fan. The current elevation of the Aravalli Mountains ranges from 600 to 900 m. However, given their long history of erosion, the Aravalli Mountains would have been considerably higher during the creation of the fans. This greater elevation would have provided ample relief for the production and transport of gravels over a distance of 200 to 300 km, allowing them to be deposited as fans. Currently, also, fractured bedrock blocks descend downhill on the western slope of the Aravalli Mountains (Figure S5).

In summary, it seems plausible to suggest that during the Miocene or earlier times, the highly elevated Aravalli mountains supplied rocks/gravels toward the sea to the west. The gravels were deposited in a fluvio-deltaic situation and thereafter were converted into conglomerates during their residence in the sedimentary basins, viz. Jaisalmer, Bikaner-Nagaur and Barmer. This is seen in the sub-surface stratigraphy of these basins, which shows multiple occurrences of gravels/conglomerates at various depths (Roy & Jakhar, 2002; Wadhawan, 1988, 2018). The deposition of parent gravels was discontinuous and has been assigned an age range of Mid Miocene to Pleistocene in the Barmer Basin; Mesozoic in the Jaisalmer Basin and Permian-Carboniferous to Pleistocene in the Bikaner-Nagaur Basin (Table S1).

Further, the matrix within the pavement gravels is dark brown sand, with rounded to subrounded granules and pebbles (Figures 3 and 4). Preliminary luminescence dating of the sandy infill, using the NCF-DSAR method (Kaushal, Chauhan, & Singhvi, 2022; Singhvi et al., 2011), suggests an age of ~30 ka, indicating that it is a secondary infill that accumulated within the gravel voids.

5.2 | Model surface exposure ages

To convert cosmogenic nuclide concentrations (Table 2) into ages, four scenarios were considered:

a. The gravels always remained on the surface. This unlikely scenario provides the absolute minimum ages.
b. The gravels experienced variable production rates due to redistribution in depth (Figure 6). For this scenario, an average burial depth of 50 cm (equivalent to a shielding factor of 0.44) was assumed to estimate an exposure age (see Figure S6).
c. The gravel surface was a constantly eroding surface with an erosion rate of 0.01 cm/ka.
d. The gravel surface was a constantly eroding surface with an erosion rate of 0.05 cm/ka).

Scenario b above is based on a simple model for the formation of the gravel spreads (Figure 6) where in the production of ^{21}Ne and ^{10}Be began at a time when the conglomerates reached a depth of a few

TABLE 2 Sample details, ^{10}Be and ^{21}Ne concentrations.

Sites	Sample	Latitude (°N)	Longitude (°E)	Elevation (m)	^{10}Be ($\times 10^6$ atoms/g)[a]		^{21}Ne$_{ex}$ ($\times 10^6$ atoms/g)[b]
Bhojka locality-1	BH1	26.953061	71.203964	207	2.21 ± 0.30		$13.2^{+1.4}_{-0.6}$
	BH2				1.42 ± 0.36		9.4 ± 1.3
Bhojka locality-2	BH-S	26.953061	71.203964	207	3.24 ± 0.15	3.27 ± 0.17	n.m.
	BH-25				3.46 ± 0.21		
	BH-50-70				3.11 ± 0.16		
Bhojka locality-3	BHCONG	26.961939	71.228288	207	5.55 ± 0.44		n.m.
Hamira	HMCRN1	26.989890	71.089843	200	4.43 ± 0.48		$14.9^{+2.1}_{-1.8}$
Solanki	SGCRN1	26.015971	70.802634	210	3.19 ± 0.42		$20.8^{+2.3}_{-1.9}$
Jayal	JKCRN1	27.243889	74.286764	320	2.63 ± 0.30		$20.9^{+2.6}_{-2.4}$

[a] ^{10}Be concentrations are normalized to standard sample SRM 4325 (nominal ^{10}Be/^{9}Be ratio: 2.79×10^{-11}). ^{10}Be/^{9}Be ratios were corrected by a full chemistry procedural blank. Error limits are 1σ.
[b] Cosmogenic ^{21}Ne concentrations (Table S3) with 1σ error limits.
n.m.: not measured.

metres from their ambient surface. Thereafter they were continually exposed to cosmic rays, with production rates determined by their depth. The region was likely traversed by aeolian sediments at times, which could have attenuated or completely stopped the production of ^{10}Be and ^{21}Ne. During periods of no production, the concentration of stable ^{21}Ne would have remained unchanged, whereas the ^{10}Be concentration would have declined at a rate governed by its half-life. Thus, the combination of ^{21}Ne and ^{10}Be helps to estimate an upper bound to the exposure ages (obtained from ^{21}Ne) and the possible impact of sediment overburden, expressed in a ^{10}Be and ^{21}Ne age difference.

It can reasonably be assumed that any ^{10}Be produced in the gravels during their residence on the Aravalli Mountains or during travel and deposition at the sites (i.e. from the Mesozoic till the recent re-exposure by denudation) would have decayed during sediment

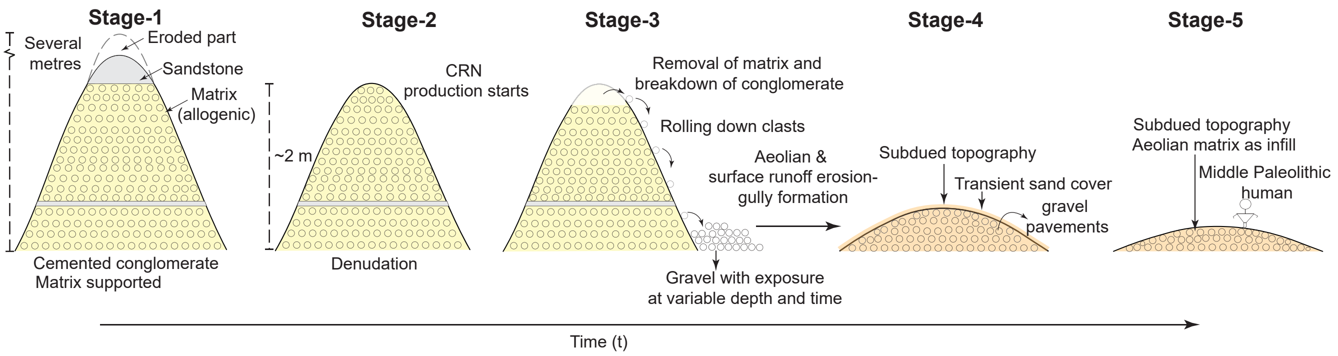

FIGURE 6 Schematic illustrating the evolution of gravel pavement surfaces and a broad event sequence that may be responsible to build up ^{10}Be and ^{21}Ne in quartz clasts. The following event sequence is considered: Stages 1 and 2: The conglomerate surface was a buried undulating surface of a palaeofan. Over time, the surface was denuded and this process continued until the conglomerates were within the top few metres of the local surface, allowing quartz within them to accumulate cosmic ray-produced ^{21}Ne and ^{10}Be. Stage 3: concurrent to the cosmic ray exposure, a gradual loss of matrix and disintegration of the conglomerate into gravels occurred, due to mechanical weathering, facilitated by temperature change and wetting-drying cycles. Aeolian activity winnowed finer fractions and surface runoff processes formed rills and gullies that also removed the matrix. On disintegration, gravels moved down-slope with gravity, exposing the members beneath them to cosmic ray exposure, and this disintegration process continued until slopes became smooth. Stage 4. The disintegration and a random distribution of clasts obliterated primary gravel imbrication structures. Stage 5. After this, the voids between gravel clasts were filled by sand/silt and calcrete developed.

TABLE 3 ^{10}Be and ^{21}Ne modelled surface exposure ages as obtained by considering various possible depth and erosion rate scenarios.

		On surface (production 100%)		Average depth of 50 cm (partial burial)		On surface production 100%		On surface production 100%	
						Erosion = 0.01 cm/ka		Erosion = 0.05 cm/ka	
		S = 1		S = 0.44		S = 1		S = 1	
-Sites	Sample	^{10}Be model exposure age (ma)[a]	^{21}Ne model exposure age (ma)[a]	^{10}Be model exposure age (ma [a]	^{21}Ne model exposure age (ma)[a]	^{10}Be model exposure age (ma)[a]	^{21}Ne model exposure age (ma)[a]	^{10}Be model exposure age (ma)[a]	^{21}Ne model exposure age (ma)[a]
Bhojka locality-1	BH1	0.69 ± 0.11	$0.80^{+0.08}_{-0.04}$	2.10 ± 0.48	$1.82^{+0.19}_{-0.09}$	0.74 ± 0.13	$0.86^{+0.10}_{-0.05}$	1.12 ± 0.34	$1.31^{+0.25}_{-0.12}$
	BH2	0.42 ± 0.12	0.57 ± 0.08	1.11 ± 0.37	1.30 ± 0.17	0.44 ± 0.13	0.60 ± 0.08	0.53 ± 0.19	0.77 ± 0.14
Bhojka locality-2	BH-S, BH-25, BH-50-70	1.13 ± 0.08	*n.m.*	5.4 ± 1.2	*n.m.*	1.28 ± 0.10	*n.m.*	*Saturated	*n.m.*
Bhojka locality-3	BHCONG	2.51 ± 0.37	*n.m.*	*Saturated	*n.m.*	4.3 ± 1.7	*n.m.*	*Saturated	*n.m.*
Hamira	HMCRN1	1.74 ± 0.29	$0.91^{+0.13}_{-0.11}$	*Saturated	$2.06^{+0.29}_{-0.26}$	2.18 ± 0.51	$0.98^{+0.15}_{-0.13}$	*Saturated	$1.67^{+0.52}_{-0.45}$
Solanki	SGCRN1	1.11 ± 0.19	$1.28^{+0.14}_{-0.12}$	5.2 ± 2.8	$2.92^{+0.32}_{-0.27}$	1.23 ± 0.25	$1.42^{+0.18}_{-0.15}$	*Saturated	*Saturated
Jayal	JKCRN1	0.76 ± 0.10	$1.15^{+0.14}_{-0.13}$	2.43 ± 0.50	$2.62^{+0.33}_{-0.30}$	0.94 ± 0.12	$1.42^{+0.18}_{-0.16}$	1.88 ± 0.43	*Saturated

[a]Exposure ages are calculated using scaling factors derived from Lal (1991). ^{10}Be and ^{21}Ne modelled exposure ages have error limits of 1σ. Uncertainties in production rates and shielding factors were not considered.
*Sample appears to be saturated (i.e., measured concentration is higher than the maximum concentration attainable in this scenario) at this erosion rate or shielding depth. See section 4.3 for model assumptions.
n.m.: not measured.

storage at a depth of a few hundred metres over a few tens of millions of years. In contrast, stable ^{21}Ne would have remained unchanged. Consequently, similar ^{10}Be and ^{21}Ne model exposure ages would imply an absence of inherited Ne, while a difference in Be and Ne ages would suggest a phase of shielding due to overburden or inheritance from the source area or during transport.

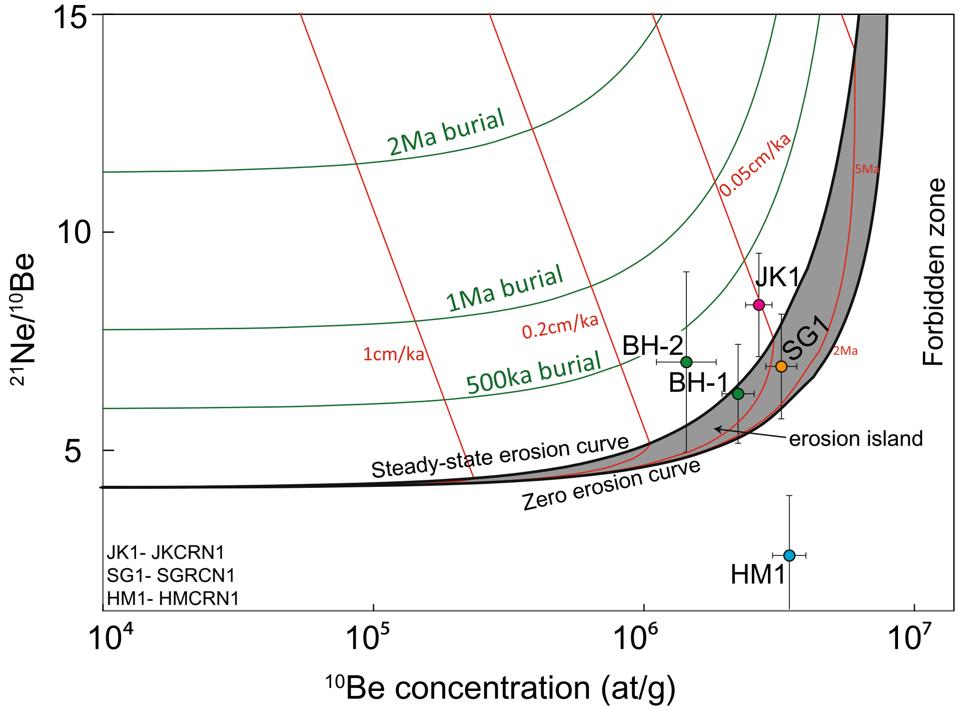

FIGURE 7 ^{21}Ne/^{10}Be two-nuclide (or erosion island) plot for gravel spread samples of the Thar Desert. The "erosion island" (denoted by a filled grey colour between bold lines) represents the possible location of data points of samples with a single-stage exposure and erosion history. Two of our samples (BH-1 and SGCRN1) plot inside the steady-state erosion island, while two more samples (BH-2 and JKCRN1) plot slightly above it, indicating some burial signals or inheritance of ^{21}Ne. However, sample HMCRN1 plots below the "zero erosion" line, falling in the forbidden zone, which may indicate some analytical issues. The green colour lines are isochrons of burial/shielding duration assuming a simple burial history after complete nuclide saturation. This two-nuclide diagram is plotted in CosmoCalc v–3.0 (Vermeesch, 2007) and uses (1) SLHL production rates according to section 4.3, (2) 1σ errors for both nuclides, (3) ^{21}Ne/^{10}Be ratio (on y-axis) is plotted at linear scale (4) CosmoCalc default assumptions for all other parameters.

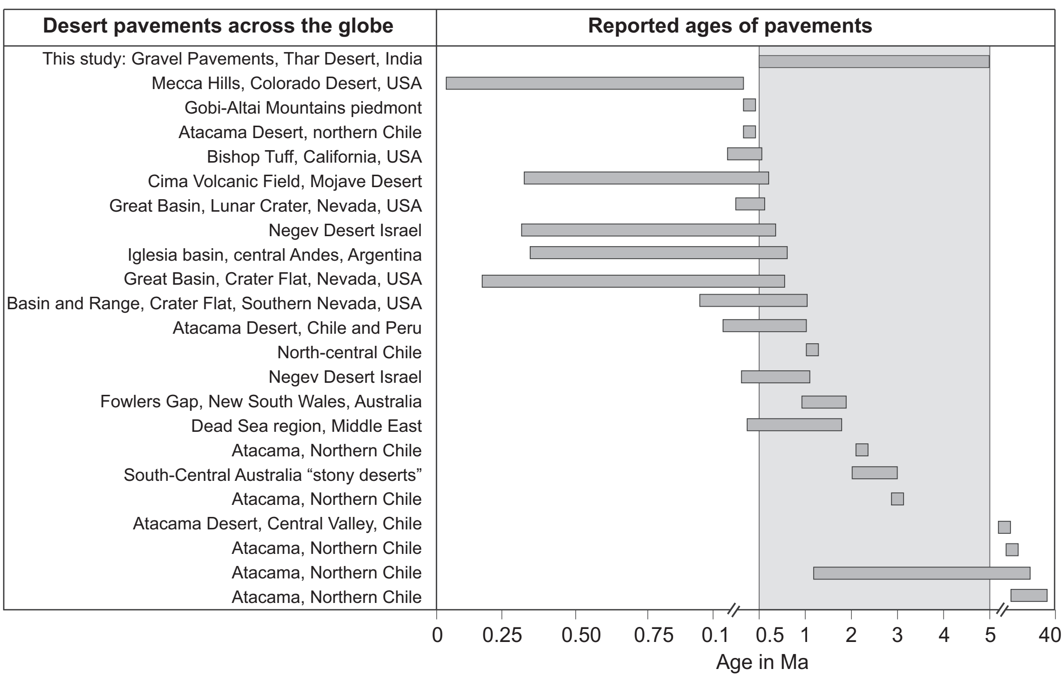

FIGURE 8 Exposure ages of gravel pavements of the Thar Desert (denoted by grey band) are compared with the reported ages of selected desert pavement surfaces across the globe. The global data on desert pavement ages are sourced from Seong, Dorn, & Yu (2016).

The presence of artefacts of successive Palaeolithic cultural phases on the surfaces of the gravel pavements (Misra, 2007) suggests that the pavement topography remained relatively unchanged with respect to tectonics.

Table 3 provides the ages under the four scenarios described above, viz. gravels on the surface, gravels with an average burial depth of 50 cm and gravels that eroded at rates of 0.01 cm/ka or 0.05 cm/ka. The first scenario provides minimum ages. The assumption of partial burial (with an average burial depth of 50 cm) provides more realistic ages as it accounts for cosmic ray exposure during exhumation of the conglomerate, its residence on the surface, gravity sliding and residence thereafter till the present. For the third and fourth scenarios, the exposure ages were obtained for two possible erosion rates 0.01 and 0.05 cm/ka. For erosion rates above 0.05 cm/ka, the measured ^{10}Be and ^{21}Ne concentrations are higher than the maximum concentrations that can be achieved in erosion equilibrium. Such rates are unrealistic in our setting. Taken together, the data provide a set of ages ranging from ~1 to 5 Ma. The discussion below uses ages based on scenario b for gravels with an average burial depth of 50 cm.

The ^{10}Be concentrations are in the range of 1.42 to 5.55 × 10^6 atoms/g and ^{21}Ne concentrations vary from 9.4 to 20.9 × 10^6 atoms/g. At Bhojka, ^{10}Be ages span a time of 1.11–2.10 Ma at locality 1 (samples BH1 and BH2) and ~5.4 Ma at locality 2. ^{21}Ne ages for locality 1 range from 1.30 to 1.82 Ma. At locality 2, three samples (BH-S, BH-25 and BH-50-70) from the surface down to 60 ± 10 cm depth were measured for ^{10}Be only. The similarity of ^{10}Be concentrations irrespective of depth (Figure S7) suggests random mixing of the gravels due to gravity sliding. Conglomerate sample BHCONG from Bhojka provided a saturated ^{10}Be signal, corresponding to an age of >5 Ma, which is consistent with geological reasoning suggesting that the tectonic exhumation occurred before 5 Ma.

The sample from Hamira (HMCRN-1) yields a saturated ^{10}Be concentration as well, corresponding to an age of >5 Ma, whereas the ^{21}Ne exposure age is only 2.06 Ma. This anomaly will be examined in the future, but here we use the present Ne age of 2.06 Ma as a working estimate. Model exposure ages at Solanki (SGCRN-1) are ~5.2 Ma for ^{10}Be and 2.92 Ma for ^{21}Ne, suggesting that the measured ^{10}Be concentration is close to saturation. Sample JKCRN-1 from Jayal gave a ^{10}Be exposure age of 2.43 Ma and a ^{21}Ne age of 2.62 Ma.

Figure 7 provides a two-nuclide plot of ^{10}Be and ^{21}Ne data. In accordance with the discussion above, samples SGCRN1 and BH1 plot inside the steady-state erosion island, which suggests a simple exhumation history, with ^{10}Be and ^{21}Ne concentrations at erosion equilibrium under a denudation rate of ~0.05 cm/ka. Samples BH2 and JKCRN1 plot nominally above the steady-state erosion island (though within error they are consistent with steady-state erosion), suggesting intermittent burial over a few hundred ka, which could be due to a transient overburden such as mobile dunes. Alternatively, an inherited ^{21}Ne component from exposure in the source area or during transport is possible. Sample HMCRN1 is in the forbidden zone due to low ^{21}Ne and high ^{10}Be. The reason for that is not clear.

To summarize, cosmogenic ^{10}Be and ^{21}Ne exposure ages are generally similar. Any burial signal in these samples could be attributed to overburden from a transiting sand dune or an inherited Ne component. ^{21}Ne ages provide an upper bound and ^{10}Be ages provide a similar time bracket of 1.11–5.4 Ma. The conglomerate sample BHCONG has a minimum age of 2.51 Ma based on ^{10}Be surface production, but could be >5 Ma if it did not stay at the very surface during its whole exposure history.

5.3 | Consistent timing of desert pavements

Seong, Dorn, & Yu (2016) collated global data on desert pavement ages which span a period from 37 Ma to 3 ka (Figure 8). It is noteworthy that in most deserts, gravel ages in the range of 3–0.5 Ma are found, including the present data from the Thar. Global cooling and aridification from 3.6 Ma onwards have been suggested (Fang et al., 2020), and the similarity of desert pavement formation ages in the Thar with the Global data is perhaps a manifestation of global desiccation events. This suggestion and causal connections of the Thar with global aridity from 3.6 Ma should be investigated further.

It has been suggested that the gravels predate the arrival of hominins, and constitute a source of raw materials for stone tool manufacture, continuing over the Pleistocene (see Misra et al., 1980). A mention of Acheulian artefacts (Misra et al., 1982) discovered in situ within the Jayal gravels offers a rare prospect of exploring an early hominin presence, although this requires further confirmation, along with the direct dating of stone artefacts.

6 | CONCLUSIONS

Using stable ^{21}Ne and radioactive ^{10}Be as cosmogenic nuclides, this study reports model exposure ages of the desert pavement in the Thar. The gravel exposure ages range from ~1 Ma to ~5 Ma. Two-nuclide plots suggest simple exposure histories, minimal inheritance and perhaps occasional episodes of burial by transiting aeolian sands. It is also noteworthy that exposed desert pavements were probably formed in response to regional/global climate cooling, and this hypothesis will be pursued.

The desert pavement ages reported here confirm previous suggestions of desertic conditions in the Thar since 1.77 Ma, and the minimum age of the conglomerate sample BHCONG of 2.51 Ma suggests that desertic conditions in the Thar existed at least during the entire Quaternary and perhaps began somewhat earlier. The archaeological significance of these dates lies in providing a baseline for the earliest Palaeolithic occupation of the region, which potentially continued both during the last phase of desert pavement formation and subsequently during phases of conducive climates. The establishment of the age of the artefacts and correlation with the desert pavement gravels studied here would be significant in exploring debates on the earliest occupation of the Thar desert and implications for hominin migrations out of Africa and across Asia.

AUTHOR CONTRIBUTIONS

AKS initiated the program. RK, SP, RJW and AKS collected the samples. RK, SP, AKS and RJW provided the geomorphic framework. RK and AKS developed the geological framework. The samples were

processed for analysis at IUAC and age calculations were carried out by RK. RK wrote the first draft and developed a conceptual model for the age calculations. PK and PVK measured Be isotopes in AMS and SN measured the Ne isotopes. SM and SP contributed to discussions on the archaeological record. The manuscript was critically commented upon by all the authors and all agreed to version is presented.

ACKNOWLEDGEMENTS

AKS thanks the Department of Science and Technology- Scientific and Engineering Research Board (DST-SERB) for the Year of Science Chair Professorship (DST-YOSCP grant no. SR/S9/YSCP-03/2019) and the Director, Physical Research Laboratory for hosting this grant. The authors thank the Inter-University Accelerator Centre for Accelerator Mass Spectrometry under the Ministry of Earth Science (MoES), Govt. of India MoES/16/07/11(i)-RDEAS and MoES/P.O. (Seismic)8(09)-Geochron/2012 grants for National Geochronology Facility. We thank Dr. Amal Kar for help in the field. Enzio Schnabel kindly carried out the noble gas analyses. We thank Dr. S. Dey for useful discussions and Dr. Naveen Chauhan for the use of the luminescence laboratory.

The contribution is respectfully dedicated to the memory of *Prof. S. N. Rajaguru, Prof, V.N. Misra and Prof. R.P. Dhir* for their pioneering contributions to the geological, geoarchaeological and pedological studies in the Thar.

We thank Dr. Michal Ben-Israel, an anonymous reviewer, the Associate Editor and the Editor, Prof. Stuart Lane for their insightful reviews that have greatly improved the paper.

CONFLICT OF INTEREST STATEMENT

The authors declare that they have no known competing financial interests or personal relationships that could have appeared to influence the work reported in this paper.

DATA AVAILABILITY STATEMENT

The data used in this paper will be provided by the corresponding author upon reasonable request.

ORCID

Rahul K. Kaushal https://orcid.org/0000-0002-5014-1798

REFERENCES

Adelsberger, K.A., Smith, J.R., McPherron, S.P., Dibble, H.L., Olszewski, D.I., Schurmans, U.A., et al. (2013) Desert pavement disturbance and artifact Taphonomy: a case study from the eastern Libyan plateau, Egypt. *Geoarchaeology*, 28(2), 112–130.

Agrawal, D.P., Dutta, P.S., Hussain, Z., Krishnamurthy, R.V., Misra, V.N., Rajaguru, S.N., et al. (1980) Palaeoclimate, stratigraphy and prehistory in north and West Rajasthan. *Proceedings of the Indian Academy of Sciences*, 89, 51–66.

Akhilesh, K., Pappu, S., Rajapara, H.M., Gunnell, Y., Shukla, A.D. & Singhvi, A.K. (2018) Early Middle Palaeolithic culture in India around 385–172 ka reframes out of Africa models. *Nature*, 554(7690), 97–101. Available from: https://doi.org/10.1038/nature25444

Allchin, B., Goudie, A. & Hegde, K.T.M. (1978) *The prehistory and palaeogeography of the great Indian Desert*. London: Academic Press.

Amit, R., Simhai, O., Ayalon, A., Enzel, Y., Matmon, A., Crouvi, O., et al. (2011) Transition from arid to hyper-arid environment in the southern Levant deserts as recorded by early Pleistocene cumulic Aridisols. *Quaternary Science Reviews*, 30(3–4), 312–323.

Anderson, R.S., Repka, J.L. & Dick, G.S. (1996) Explicit treatment of inheritance in dating depositional surfaces using in situ ^{10}Be and ^{26}Al. *Geology*, 24(1), 47–51.

Anil, D., Chauhan, N., Ajithprasad, P., Devi, M., Mahesh, V. & Khan, Z. (2022) An early presence of modern human or convergent evolution? A 247 ka middle Palaeolithic assemblage from Andhra Pradesh, Egypt. *Journal of Archaeological Science: Reports*, 45, 103565.

Bajpai, V.N. (2004) Hydrogeological evolution of the Luni River basin, Rajasthan, western India: a review. *Journal of Earth System Science*, 113, 427–451.

Bakliwal, P.C. & Grover, A.K. (1988) Signatures and migration of Saraswati River in the Thar Desert. *Records of the Geological Survey of India*, 116, 3–8.

Bakliwal, P.C. & Wadhawan, S.K. (2003) Geological evolution of Thar Desert in India —issues and prospects. *Proceedings of the Indiana Academy of Sciences*, 69A, 151–166.

Ben-Israel, M., Matmon, A., Haviv, I. & Niedermann, S. (2018) Applying stable cosmogenic ^{21}Ne to understand surface processes in deep geological time (10^7–10^8 yr). *Earth and Planetary Science Letters*, 498, 266–274.

Bhandari, A. (1999) Phanerozoic stratigraphy of Western Rajasthan Basin: A Review. Proceedings of the Seminar on Geology of Rajasthan – Status and Perspective (A.B. Roy Felicitation Volume) (Ed. P. Kataria), 126–174, Geology Dept. MLSU, Udaipur.

Biswas, R.K. & Ghosh, R.N. (1981) Periglacial and fluvioglacial landscape in the Jaisalmer district. In: Mann, H.S. (Ed.) *Arid zone Research and Development*. Jodhpur: Scientific Publishers.

Blinkhorn, J., Achyuthan, H., Durcan, J., Roberts, P. & Ilgner, J. (2021) Constraining the chronology and ecology of Late Acheulean and Middle Palaeolithic occupations at the margins of the monsoon. *Scientific Reports*, 11(1)., 19665. Available from: https://doi.org/10.1038/s41598-021-98897-7

Borchers, B., Marrero, S., Balco, G., Caffee, M., Goehring, B., Lifton, N., et al. (2016) Geological calibration of spallation production rates in the CRONUS-earth project. *Quaternary Geochronology*, 31, 188–198.

Brahmam, N.K. (1993) Gravity and seismicity of Jaisalmer region, Rajasthan. *Current Science*, 64, 837–840.

Chmeleff, J., von Blanckenburg, F., Kossert, K. & Jakob, D. (2010) Determination of the ^{10}Be half-life by multicollector ICP-MS and liquid scintillation counting. *Nuclear Instruments and Methods in Physics Research Section B: Beam Interactions with Materials and Atoms*, 268, 192–199.

Das Gupta, S.K. (1975) A revision of the Mesozoic–Tertiary stratigraphy of the Jaisalmer Basin, Rajasthan. *Indian Journal of Earth Sciences*, 2(1), 77–94.

Dhir, R.P. (1976) Palaeoclimate inferences from Quaternary pedogenetic processes in arid Zone soil. In: Agrawal, D.P. & Pande, B.M. (Eds.) *Ecology and Archaeology of Western India*. Delhi: Concept Publishing Company, Delhi, pp. 127–134.

Dhir, R.P., Joshi, D.C. & Kathju, S. (2018) *Thar Desert in retrospect and prospect*. Scientific Publishers, Jodhpur, India, p. 403.

Dhir, R.P., Kar, A., Wadhawan, S.K., Rajaguru, S.N., Misra, V.N., Singhvi, A.K., et al. (1992) *The Thar Desert in* Rajasthan. Bangalore: Geological Society of India.

Dhir, R.P. & Singhvi, A.K. (2012) The Thar Desert and its antiquity. *Current Science*, 102(7) 1001–1008.

Dhir, R.P., Singhvi, A.K., Andrews, J.E., Kar, A., Sareen, B.K., Tandon, S.K., et al. (2010) Multiple episodes of aggradation and calcrete formation in Late Quaternary aeolian sands, Central Thar Desert, Rajasthan, India. *Journal of Asian Earth Sciences*, 37(1), 10–16.

Dhir, R.P., Tandon, S.K., Sareen, B.K., Ramesh, R., Rao, T.K.G., Kailath, A.J., et al. (2004) Calcretes in the Thar Desert: genesis, chronology and palaeoenvironment. *Proceedings of the Indian Academy of Sciences (Earth Planetary Science)*, 113, 473–515.

Dolson, J., Burley, S.D., Sunder, V.R., Kothari, V., Naidu, B., Whiteley, N.P., et al. (2015) The discovery of the Barmer Basin, Rajasthan, India and its petroleum geology. *The American Association of Petroleum Geologists Bulletin*, 99, 433–465.

Dunai, T.J., López, G.A.G. & Juez-Larré, J. (2005) Oligocene–Miocene age of aridity in the Atacama Desert revealed by exposure dating of erosion-sensitive landforms. *Geology*, 33(4), 321–324.

Evenstar, L.A., Hartley, A.J., Stuart, F.M., Mather, A.E., Rice, C.M. & Chong, G. (2009) Multiphase development of the Atacama planation surface recorded by cosmogenic ^{3}He exposure ages: implications for uplift and Cenozoic climate change in western South America. *Geology*, 37(1), 27–30.

Fang, X., An, Z., Clemens, S.C., Zan, J., Shi, Z., Yang, S., et al. (2020) The 3.6-Ma aridity and westerlies history over midlatitude Asia linked with global climatic cooling. *Proceedings of the National Academy of Sciences*, 117(40), 24729–24734.

Fenton, C.R., Niedermann, S., Dunai, T. & Binnie, S.A. (2019) The SPICE project: Production rates of cosmogenic ^{21}Ne, ^{10}Be, and ^{14}C in quartz from the 72 ka SP basalt flow, Arizona, USA. *Quaternary Geochronology*, 54, 101019.

Fitzsimmons, K.E., Cohen, T.J., Hesse, P.P., Jansen, J., Nanson, G.C., May, J.H., et al. (2013) Late Quaternary paleoenvironmental change in the Australian drylands. *Quaternary Science Reviews*, 74, 78–96.

Fujioka, T. & Chappell, J. (2011) Desert landscape processes on a timescale of millions of years, probed by cosmogenic nuclides. *Aeolian Research*, 3(2), 157–164.

Fujioka, T., Chappell, J., Honda, M., Yatsevich, I., Fifield, K. & Fabel, D. (2005) Global cooling initiated stony deserts in Central Australia 2–4 ma, dated by cosmogenic ^{21}Ne–^{10}Be. *Geology*, 33, 993–996.

Gaillard, C., Mishra, S., Singh, M., Deo, S. & Abbas, R. (2010) Lower and Early Middle Pleistocene Acheulian in the Indian subcontinent. *Quaternary International*, 223, 234–241.

Ganjoo, R. K., Raghavan, H., & Raghavan, HN. Rajaguru, S.N. & Gaillard, C. (1984) Late Neogene fossil wood from Bikaner gravel bed. *Current Science*, 53(22), 1207–1208.

Ghosh, R.N. (1977) Photogeological Studies on Ancient Water Regimes of Rajasthan Rivers. In: Agrawal, D.P. & Pande, B.M. (Eds.) *Ecology and archaeology of Western India*. Delhi: Concept Publishing House, pp. 157–168.

Gosse, J.C. & Phillips, F.M. (2001) Terrestrial in situ cosmogenic nuclides: theory and application. *Quaternary Science Reviews*, 20(14), 1475–1560.

Granger, D.E. & Smith, A.L. (2000) Dating buried sediments using radioactive decay and muogenic production of ^{26}Al and ^{10}Be. *Nuclear Instruments and Methods in Physics Research, Section B: Beam Interactions with Materials and Atoms*, 172, 822–826.

Hackett, C.A. (1880) Salt in Rajputana. *Records of the Geological Survey of India*, 13, 197.

Hancock, G.S., Anderson, R.S., Chadwick, O.A. & Finkel, R.C. (1999) Dating fluvial terraces with 10Be and 26Al profiles: Application to the Wind River, Wyoming. *Geomorphology*, 27(1–2), 41–60.

Heineke, C., Hetzel, R., Nilius, N.P., Glotzbach, C., Akal, C., Christl, M., et al. (2019) Spatial patterns of erosion and landscape evolution in a bivergent metamorphic core complex revealed by cosmogenic ^{10}Be: The Central Menderes massif (western Turkey). *Geosphere*, 15(6), 1846–1868.

Jain, M. & Tandon, S.K. (2003) Fluvial response to Late Quaternary climate changes, western India. *Quaternary Science Reviews*, 22(20), 2223–2235.

Jain, M., Tandon, S.K., Singhvi, A.K., Mishra, S. & Bhatt, S.C. (2005) Quaternary alluvial stratigraphical development in a desert setting: a case study from the Luni River basin, Thar Desert of western India. *Fluvial Sedimentology VII*, 35, 349–371.

Kaila, P. & Roy, A.K. (1989) Calcareous Nanoplankton from the Jurassic Sequence off Jaisalmer, Rajasthan. In: Kalia, P. (Ed.) *Micropalaeontology of the shelf sequences of India. Proceedings of the XII Indian colloquium on Micropalaeontology and stratigraphy*. Delhi: Papyrus Publishing Company.

Kailath, A.J., Rao, T.K.G., Dhir, R.P., Nambi, K.S.V., Gogte, V.D. & Singhvi, A. (2000) Electron spin resonance characterization of calcretes from Thar Desert for dating applications. *Radiation Measurements*, 32(4), 371–383.

Kaushal, R.K., Chauhan, N. & Singhvi, A.K. (2022) Luminescence dating of quartz: a MATLAB-based program for computation of SAR paleodoses using natural sensitivity correction (NCF). *Ancient TL*, 40(2).

Knight, J. & Zerboni, A. (2018) Formation of desert pavements and the interpretation of lithic-strewn landscapes of the Central Sahara. *Journal of Arid Environments*, 153, 39–51.

Kohl, C.P. & Nishiizumi, K. (1992) Chemical isolation of quartz for measurement of in-situ-produced cosmogenic nuclides. *Geochimica et Cosmochimica Acta*, 56(9), 3583–3587.

Korschinek, G., Bergmaier, A., Faestermann, T., Gerstmann, U.C., Knie, K., Rugel, G., et al. (2010) A new value for the half-life of ^{10}Be by heavy-ion elastic recoil detection and liquid scintillation counting. *Nuclear Instruments and Methods in Physics Research Section B: Beam Interactions with Materials and Atoms*, 268, 187–191.

Lal, D. (1991) Cosmic-ray labeling of erosion surfaces: In situ nuclide production rates and erosion models. *Earth and Planetary Science Letters*, 104, 424–439.

Lü, Y., Gu, Z., Aldahan, A., Zhang, H., Possnert, G. & Lei, G. (2010) ^{10}Be in quartz gravel from the Gobi Desert and evolutionary history of alluvial sedimentation in the Ejina Basin, Inner Mongolia, China. *Chinese Science Bulletin*, 55, 3802–3809.

Matmon, A., Simhai, O., Amit, R., Haviv, I., Porat, N., McDonald, E., et al. (2009) Desert pavement-coated surfaces in extreme deserts present the longest-lived landforms on earth. *Geological Society of America*, 121, 688–697.

Mishra, S., Gaillard, C., Deo, S., Singh, M., Abbas, R. & Agarwal, N. (2010) Large flake Acheulian in India: implications for understanding Lower Pleistocene human dispersals. *Quaternary International*, 223(224), 271–272.

Misra, V.N. (1961) Palaeolithic culture of Western Rajputana. *Bulletin of the Deccan College Research Institute*, 21, 85–156.

Misra, V.N. (2006) A gazetteer of archaeological sites in Rajasthan (from Palaeolithic to Early Historic). *Man and Environment*, 31(1), 48–96.

Misra, V.N. (2007) *Rajasthan Prehistoric and Early Historic Foundations*. New Delhi: Aryan Book International.

Misra, V.N. & Rajaguru, S.N. (1989) In: Frifelt, K. & Sorensen, R. (Eds.) *Palaeoenvironments and prehistory of the Thar Desert, Rajasthan, India south Asian Archeaology - 1985*. Frifelt, K. and Sorensen, R. (Eds.), Copenhagen: Scandinavian Institute of Asian Studies Occasional Paper No.4. London: Curzon Press, pp. 296–320.

Misra, V.N., Rajaguru, S.N., Agrawal, D.P., Thomas, P.K., Hussain, Z. & Dutta, P.S. (1980) Prehistory and Palaeoenvironment of Jayal, Western Rajasthan. *Man and Environment*, 4, 19–31.

Misra, V.N., Rajaguru, S.N., Raju, D.R., Raghavan, H. & Gaillard, C. (1982) Acheulian occupation and evolving landscape around Didwana in the Thar Desert, India. *Man and Environment*, 6(72.86), 1975-1976 .

Misra, V.N., Rajaguru, S.N., Wasson, R.J., Singh, G. & Agrawal, D.P. (1979) Further light on lower Palaeolithic occupation and Palaeoenvironment in semi-arid zone of Rajasthan. *Puratattva*, 11, 11–18.

Moharana, P.C & Raja, P. (2016) Distribution, forms and spatial variability of desert pavements in arid western Rajasthan. *Journal of the Geological Society of India*, 87, 401–410. Available from: https://doi.org/10.1007/s12594-016-0408-7

Mukhopadhyay, A.K. & Ghosh, R.N. (1976) The problem of the stratigraphic position of the bap boulders, Rajasthan. *Indian Journal of Earth Sciences*, 3(2), 220–228.

Niedermann, S. (2002) Cosmic-ray-produced noble gases in terrestrial rocks: dating tools for surface processes. *Reviews in Mineralogy and Geochemistry*, 47(1), 731–784.

Niedermann, S., Bach, W. & Erzinger, J. (1997) Noble gas evidence for a lower mantle component in MORBs from the southern East Pacific rise: Decoupling of helium and neon isotope systematics. *Geochimica et Cosmochimica Acta*, 61(13), 2697–2715.

Niedermann, S., Graf, T. & Marti, K. (1993) Mass spectrometric identification of cosmic-ray-produced neon in terrestrial rocks with multiple neon components. *Earth and Planetary Science Letters*, 118(1-4), 65–73.

Nishiizumi, K., Caffee, M.W., Finkel, R.C., Brimhall, G. & Mote, T. (2005) Remnants of a fossil alluvial fan landscape of Miocene age in the Atacama Desert of northern Chile using cosmogenic nuclide exposure age dating. *Earth and Planetary Science Letters*, 237(3–4), 499–507.

Oldham, C.F. (1983) The Saraswati and the lost river of the Indian Desert. *Journal of the Asiatic Society of Bengal, NS*, 34, 76–4499.

Paddayya, K., Blackwell, B.A.B., Jhaldiyal, R., Petraglia, M.D., Fevrier, S., Chaderton, D.A. II, et al. (2002) Recent findings on the Acheulian of the Hunsgi and Baichbal valleys, Karnataka with special reference to the Isampur excavation and its dating. *Current Science*, 83(10), 641–647.

Pappu, S., Gunnell, Y., Akhilesh, K., Braucher, R., Taieb, M., Demory, F., et al. (2011) Early Pleistocene presence of Acheulian hominins in South India. *Science*, 331(6024), 1596–1599. Available from: https://doi.org/10.1126/science.1200183

Pietsch, D. & Kuhn, P. (2012) Early Holocene paleosols at the southwestern Ramlat As- Sab'atayn desert margin: new climate proxies for southern Arabia. *Palaeogeography*, *Palaeoclimatology*, *Palaeoecology*, 365, 154–165.

Rajaguru, S.N., Mishra, S. & Ghate, S. (1996) A re-interpretation of gravel spreads in the Jaisalmer region, Thar Desert, India. *Journal of Arid Environments*, 32(1), 53–58.

Repka, J.L., Anderson, R.S. & Finkel, R.C. (1997) Cosmogenic dating of fluvial terraces, Fremont River, Utah. *Earth and Planetary Science Letters*, 152(1-4), 59–73.

Roy, A.B. & Jakhar, S.R. (2002) *Geology of Rajasthan (Northwest India): Precambrian to recent*. India: Scientific Publishers, p. 421.

Sangode, S.J., Mishra, S., Naik, S. & Deo, S. (2007) Magnetostratigraphy of the Quaternary sediments associated with some Toba tephra and Acheulian artefact bearing localities in the western and Central India. *Gondwana Geological Magazine*, 10, 111–121.

Seong, Y.B., Dorn, R.I. & Yu, B.Y. (2016) Evaluating the life expectancy of a desert pavement. *Earth-Science Reviews*, 162, 129–154.

Sharma, H.S. (1987) *Tropical Geomorphology*. New Delhi: Concept Publishing Company.

Singhvi, A.K. (Ed). (2004) Quaternary history and paleoenvironmental record of the Thar Desert in India-preface. *Proceedings of the Indian Academy of Sciences-Earth and Planetary Sciences*, 113(3), 367–515.

Singhvi, A.K. & Kar, A. (Eds). (1992) *Thar Desert in Rajasthan*. Bangalore: Geological Society of India, p. 191.

Singhvi, A.K. & Kar, A. (2004) The aeolian sedimentation record of the Thar Desert. *Earth and Planetary Science*, 113, 371–401.

Singhvi, A.K., Stokes, S.C., Chauhan, N., Nagar, Y.C. & Jaiswal, M.K. (2011) Changes in natural OSL sensitivity during single aliquot regeneration procedure and their implications for equivalent dose determination. *Geochronometria*, 38, 231–241.

Singhvi, A.K., Williams, M.A.J., Rajaguru, S.N., Misra, V.N., Chawla, S., Stokes, S., et al. (2010) A~ 200 ka record of climatic change and dune activity in the Thar Desert, India. *Quaternary Science Reviews*, 29(23–24), 3095–3105.

Sinha Roy, S. (1986) Himalayan collision and indentation of the Aravalli orogen by Bundelkhand wedge: implications for neotectonics in Rajasthan. In: *Proceedings of international symposium on Neotectonics in South Asia*. Dehradun: Survey of India, pp. 18–21.

Sinha Roy, S., Malhotra, G. & Mohanty, M. (1998) *Geology of Rajasthan*. Geological Society of India, p.278.Bangalore, India.

Sisodia, M.S. & Singh, U.K. (2000) Depositional environment and hydrocarbon prospects of the Barmer Basin, Rajasthan, India. *Nafta*, 51, 309–326.

Tiwari, O.N. (1992) Fallibility of palaeo-Tchannels as groundwater potential zones in a part of the Thar Desert. *Journal of the Geological Society of India*, 40, 70–75.

Vermeesch, P. (2007) CosmoCalc: An Excel add-in for cosmogenic nuclide calculations. *Geochemistry, Geophysics, Geosystems*, 8(8).

Wadhawan, S.K. (1988) Evolution of Quaternary aeolian deposits of Jodhpur and Barmer districts, Rajasthan, India. In: Patel, M.P. & Desai, N. (Eds.) *Proceedings, National Seminar on recent quaternary studies in India*. Baroda: M.S. University, pp. 64–78.

Wadhawan, S.K. (2018) Palaeogene–Neogene tectonics and continental aggregational basins in north-western India: Implications for geological evolution of Thar Desert. In: *The Indian Paleogene*, pp. 151–166.

Wang, F., Michalski, G., Seo, J.H., Granger, D.E., Lifton, N. & Caffee, M. (2015) Beryllium-10 concentrations in the hyper-arid soils in the Atacama Desert, Chile: implications for arid soil formation rates and El Niño driven changes in Pliocene precipitation. *Geochimica et Cosmochimica Acta*, 160, 227–242.

SUPPORTING INFORMATION

Additional supporting information can be found online in the Supporting Information section at the end of this article.

How to cite this article: Kaushal, R.K., Parida, S., Kumar, P.V., Kumar, P., Niedermann, S., Wasson, R.J. et al. (2024) Cosmogenic ^{10}Be- and ^{21}Ne-based model exposure ages of desert pavements in the Thar Desert, India. *Earth Surface Processes and Landforms*, 1–15. Available from: https://doi.org/10.1002/esp.5999